ASSESSMENT OF EUTROPHICATION RISKS IN BLACK-ODOR WATER BODIES BASED ON SENTINEL-2 IMAGERY AND KDE-VINE COPULA: A CASE STUDY OF CHANGCHUN, CHINA

YAO, G. Y.[1] – MA, J.[1*] – SHAO, Y. X.[1] – BI, Q.[2]

[1]*Changchun Institute of Technology, School of Prospecting & Surveying Engineering, Changchun 130012, China*
(e-mail: yaoguanyu@stu.ccit.edu.cn (Yao, G. Y.); shaoyaxuan@stu.ccit.edu.cn, (Shao, Y. X.))

[2]*Jilin Hydropower Planning & Design Institute, Changchun 130012, China*
(e-mail: gis753@163.com)

[*]*Corresponding author*
e-mail: kc_mj@ccit.edu.cn

(Received 7th May 2025; accepted 10th Jul 2025)

Abstract. Fast industrialization in developing countries has deteriorated urban water quality, and the assessment of aquatic ecological environment quality is becoming challenging. In this study, separability and thresholds (SEaTH), integrated with Vector Machine (SVM) was applied based on Sentinel-2 imagery for the identification of black-odor water bodies in several typical water bodies in Changchun City, China. A eutrophication risk assessment model for black-odor water bodies based on KDE (Kernel Density Estimation, KDE)-Vine Copula was proposed, integrated with Geographic Detector analysis. The results showed that from 2017 to 2019, the maximum value of Chlorophyll-a (Chl-a) in the typical water bodies decreased from 42.60 μg/L to 38.07 μg/L, and the Total Suspended Solids (TSS) content decreased from 208.20 mg/L to 198.27 mg/L, indicating a general reduction in degree of eutrophication. The highest risk probabilities in 2017-2019 were 44.41%, 34.96%, and 51.73%, respectively. Significant progress in the restoration of water ecological functions was observed in 2018, while the water ecological quality declined in 2019. According to the Geographic Detector results, TSS had a stronger explanatory power on eutrophication. However, the interaction between TSS and factors with weaker explanatory power, such as Chl-a and Secchi Depth (SD), did not significantly enhance the explanatory effect.
Keywords: *remote sensing, risk assessment, Vine Copula, geographic detector, kernel density estimation, separability and thresholds*

Introduction

Eutrophication refers to the process in which large amounts of substances that enhance biological growth enter water bodies, increasing the productivity of the aquatic ecosystem and leading to water quality deterioration (Njock et al., 2023; Pannard et al., 2024). With urban industrialization, the discharge of organic-rich wastewater inevitably pollutes urban rivers, causing secondary disasters such as eutrophication (Hei et al., 2024). This leads to the overload of the river's self-purification capacity, accelerating water quality deterioration, as well as hindering the construction of aquatic ecosystems (Cheng et al., 2024). Therefore, controlling the degree of eutrophication in water bodies is a necessary stage in urban river management, and water quality monitoring is an essential component for the management of urban aquatic environment (Barzegar et al., 2020).

Satellite remote sensing for water quality monitoring offers several advantages, such as cost-effectiveness and high efficiency, thereby providing a novel technological approach for urban water quality surveillance. Remote sensing technology has facilitated both domestic and international research into the formation, impacts, assessment, and

http://www.aloki.hu ● ISSN 1589 1623 (Print) ● ISSN 1785 0037 (Online)
DOI: http://dx.doi.org/10.15666/aeer/2305_90759099

management of water eutrophication (Carstens and Amer, 2019; Sun et al., 2024). Li et al. (2006) conducted in-situ water quality sampling and ground spectral measurements at 21 fixed monitoring stations in Taihu Lake. Based on the empirical data, an empirical model was developed, and the nutrient status index at sampling locations was calculated to assess water eutrophication. However, ground-based measurements involve substantial labor and low efficiency, which hinder effective water quality monitoring. To mitigate these issues, unmanned aerial vehicle (UAV)-borne multispectral remote sensing technology has been adopted to enhance monitoring efficiency (Wang et al., 2025). Current research on water eutrophication assessment primarily focuses on nutrient status index evaluation. Zhao et al. (2020) analyzed the spatiotemporal variations of various physicochemical parameters, employing the Comprehensive Trophic Level Index to evaluate Baihua Lake. Li et al. (2024) applied Carlson's trophic state index to assess the eutrophication degree of reservoir water bodies. In addition to nutrient status indices, certain scholars (Wang et al., 2017) have utilized mathematical statistics, analytic hierarchy processes, and other methodologies to assess the ecological risks of Dongting Lake, considering factors such as algal biomass and shoreline morphology in constructing a risk assessment framework for blue-green algal bloom accumulation (Qian et al., 2022). These studies, which integrate empirical models with multiple index approaches and risk assessment systems, contribute to the enrichment of methods for assessing water eutrophication. Furthermore, some scholars have employed cumulative probability density models based on water quality monitoring data to predict eutrophication risks (Biggs, 2000; Azevedo et al., 2015; Brito et al., 2024). Additionally, the primary driving factors behind water eutrophication have been investigated, with geographic detectors being used to quantify the influence of these driving forces (Zhang et al., 2025), thereby offering valuable insights for the protection and management of aquatic environments.

Existing studies focus on evaluating the eutrophication degree of water bodies using composite indices. The Vine Copula function is a mathematical model that connects multivariate distributions (Czado and Nagler, 2022). It has been widely used in risk assessment research. Applications include financial investment risk, flood recurrence (Tosunoglu et al., 2020), precipitation analysis (Cantet and Arnaud, 2014; Luo et al., 2024), drought monitoring (Hasan and Abdullah, 2022; Kanthavel et al., 2022; Li et al., 2024; Meimandi, et al., 2024), and chemical process monitoring (Bhatti and Do, 2019). However, research on the application of Vine Copula functions in remote sensing water quality monitoring and eutrophication risk assessment is relatively limited. The Vine Copula function is effective in characterizing the joint distribution probability of variables. Therefore, the aim of this study is to develop a KDE-Vine Copula model by integrating remote sensing-based water quality monitoring with the Vine Copula function, utilizing kernel density estimation to reconstruct the marginal distributions in a non-parametric manner. This model is applied to assess the eutrophication risk of black-odor water bodies in Changchun. Additionally, the Geographical Detector is employed to quantify the explanatory power of various water quality parameters on the Comprehensive Trophic Level Index. This study not only provides support for water environment protection and management in Changchun but also offers a novel approach for remote sensing water quality monitoring and eutrophication evaluation.

Study area

Changchun City, located in the northeast of China, is one of the central cities in the region and a major industrial base in the country. As a result, the water quality in the

http://www.aloki.hu ● ISSN 1589 1623 (Print) ● ISSN 1785 0037 (Online)
DOI: http://dx.doi.org/10.15666/aeer/2305_90759099

urban areas has not been significantly improved. In 2017, the General Office of the Jilin Provincial Party Committee issued the "Implementation Plan for the Comprehensive Promotion of the River Chief System in Jilin Province," gradually restoring the functions of aquatic ecosystems. The Yitong River, which belongs to the Songhua River Basin, is the main river running through the urban area of Changchun from south to north. Within its basin are urban parks such as the Nanxi Wetland. However, there has been insufficient systematic planning, and the construction of water environment infrastructure such as drainage outlets has lagged behind. Consequently, typical water bodies such as the Yongchun River, Fuyu River, North Lake, and Leijia Ditch have experienced water quality deterioration, damaging the ecological functions of wetland parks, and the water ecological environment faces severe challenges. This study conducts eutrophication assessment and analysis of the typical water areas in the Yitong River basin, including North Lake, Leijia Ditch, Yongchun River, and Fuyu River, from 2017 to 2019, as shown in *Fig. 1*.

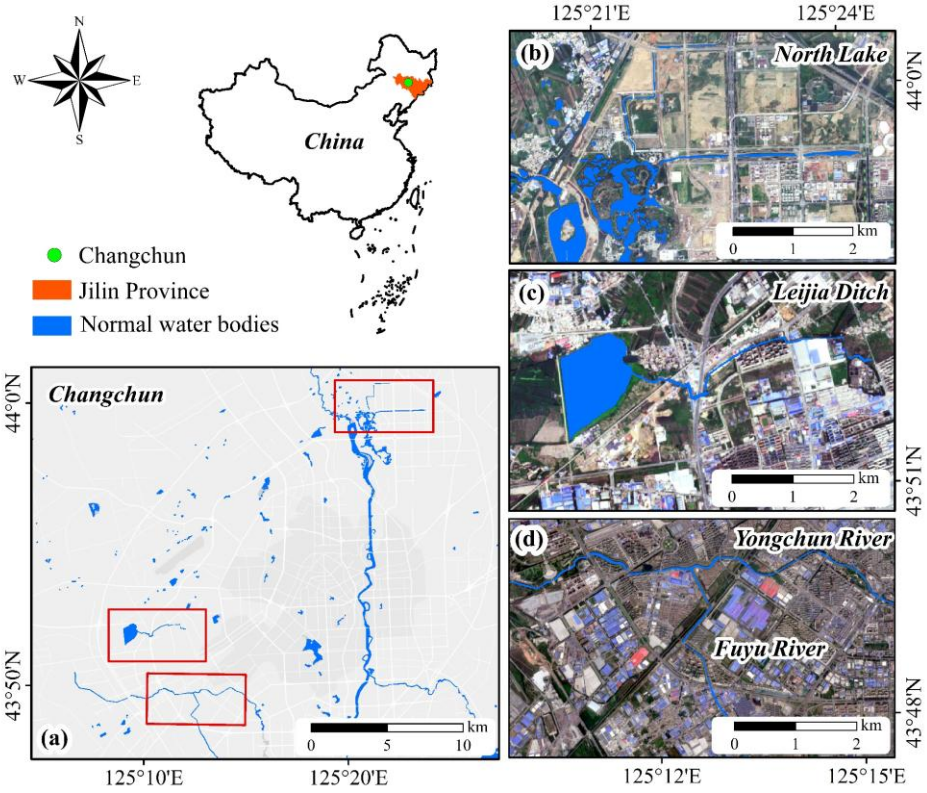

Figure 1. *Geographical location of the Yitong River basin in the central urban area of Changchun City. The North Lake, Leijia Ditch, Yongchun River, and Fuyu River were selected as typical water bodies for a study on eutrophication*

Data and methods

Data sources

Sentinel-2 is a high-resolution multispectral imaging satellite under the European Space Agency's "Copernicus Program". It consists of two polar orbiting satellites, Sentinel-2A and Sentinel-2B, equipped with a multispectral imager (MSI) that covers 13 spectral bands. The ground resolution can reach up to 10 meters, and it revisits the

http://www.aloki.hu ● ISSN 1589 1623 (Print) ● ISSN 1785 0037 (Online)
DOI: http://dx.doi.org/10.15666/aeer/2305_90759099

equatorial region of earth every five days. In this study, Sentinel-2 summer images from June 28, 2017, July 23, 2018, and June 18, 2019, were selected. The SEaTH algorithm, combined with Vine Copula and Geographic Detector, was used to assess eutrophication risk and conduct explanatory power analysis for typical black-odor water bodies in the urban area of Changchun City, as shown in *Fig. 2*.

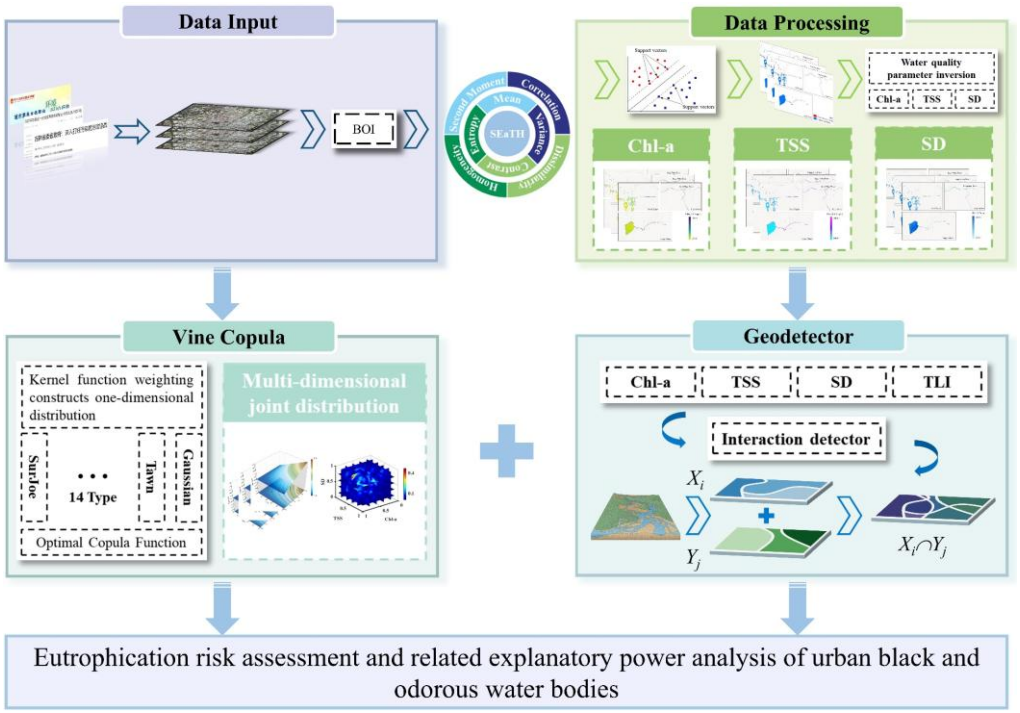

Figure 2. *Flowchart of risk assessment and interpretability analysis. The BOI refers to the brown water index. The Chl-a, TSS, and SD denote chlorophyll-a, total suspended solids, and secchi depth, respectively. In this study, the Vine Copula and Geographic Detector are employed as the primary analytical methods to assess the eutrophication risk of black and odorous water bodies. Additionally, Geographic Detector is used to quantify the explanatory power of water quality parameters on the Comprehensive Trophic Level Index (TLI)*

Construction of Black-odor water body index

General water bodies and urban black-odor water bodies exhibit different spectral characteristics across various bands. General water bodies have a significantly higher reflectance in the green band compared to the red and blue bands. In contrast, black-odor water bodies, due to higher suspended matter concentrations, exhibit a slightly higher reflectance in the red band compared to the blue band, with overall variations being relatively smooth.

The recognition model based on remote sensing reflectance enhances the spectral characteristic differences between general water bodies and black-odor water bodies, thereby improving the model's accuracy. Wen proposed the Normalized Difference Brown Water Index (NDBWI), which effectively utilizes the reflectance differences between the red and green bands to identify urban black-odor water bodies (Wen et al., 2018). Yao extended the normalized difference index by adding the blue band to construct the Brown Water Index (BOI), maximizing the reflectance difference between the red and green bands (Yao et al., 2019).

http://www.aloki.hu ● ISSN 1589 1623 (Print) ● ISSN 1785 0037 (Online)
DOI: http://dx.doi.org/10.15666/aeer/2305_90759099

SEaTH feature optimization

The SEparability and Thresholds (SEaTH) algorithm was originally applied to the detection and monitoring of nuclear facilities by the International Atomic Energy Agency (IAEA) and has gradually been extended to information extraction from remote sensing images (Qu et al., 2024). Due to the large number of feature quantities involved in remote sensing image extraction, it is crucial to reasonably select features and adopt comprehensive feature extraction methods as prerequisites for successfully processing remote sensing images, as shown in *Fig. 3*. Therefore, it is necessary to identify the importance of features, construct a feature space for data dimensionality reduction, and thus achieve feature optimization.

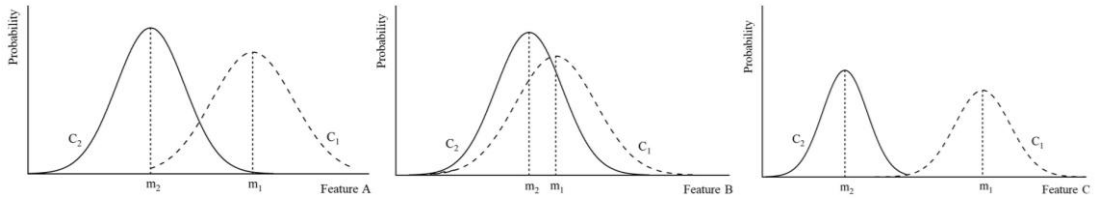

Figure 3. *Degree of separation between C_1 and C_2. C_1 and C_2 represent two distinct categories. The m_1 and m_2 denote the means of a particular feature for the two categories. The SEaTH algorithm based on categorical sample feature values uses separability to evaluate the degree of association between two categories for a given feature. The separability between categories C_1 and C_2 based on features A, B, and C is represented as partial separation, poor separation, and complete separation, respectively. This indicates that feature C is the most effective in distinguishing between categories C_1 and C_2*

In the SEaTH algorithm, the J-M (Jeffries-Matusita) distance is commonly used to measure the separability of samples. When $J = 0$, it indicates that the two categories are almost completely mixed on a given feature, with poor separability. The larger the value, the better the separability between the two categories for that feature. As shown in *Eq.1* and *Eq.2*:

$$J=2(1-e^{-B}), \quad \text{(Eq.1)}$$

$$B=\frac{1}{8}(m_1-m_2)^2\frac{2}{\sigma_1{}^2+\sigma_2{}^2}+\frac{1}{2}\ln\left[\frac{\sigma_1{}^2+\sigma_2{}^2}{2\sigma_1\sigma_2}\right], \quad \text{(Eq.2)}$$

where B represents the Bhattacharyya distance, m_1 and m_2 are the means of a particular feature for the two categories, and σ_1 and σ_2 are the standard deviations of that feature for the two categories. The SEaTH algorithm measures the separability between pairs of categories based on a certain feature. Typically, the feature corresponding to the maximum J-M distance between two categories is selected as the best feature.

Water quality parameter inversion

Remote sensing water quality monitoring offers advantages such as large coverage, all-weather capability, and high efficiency. However, real-time data for large-scale water quality monitoring is difficult to obtain. Therefore, developing highly applicable and specific inversion models has become a challenge in remote sensing water quality

http://www.aloki.hu ● ISSN 1589 1623 (Print) ● ISSN 1785 0037 (Online)
DOI: http://dx.doi.org/10.15666/aeer/2305_90759099

monitoring. As shown in *Table 1*, based on the existing empirical models developed by numerous scholars, this study selects and filters models using the Kendall correlation coefficient to examine the relationships between various indicators, applying them to water quality parameter inversion.

Table 1. *Empirical model for water quality parameters*

Parameters	Model form	Reference model
Chl-a I	$4.089(NIR/R)^2$-0.746(NIR/R)+29.733	(Zhu et al., 2015)
Chl-a II	72.632VNIR2(1/R - 1/VNIR1)+4.9605	(Dall et al., 2005; Li et al., 2022)
Chl-a III	28.958(G/B)+9.34(NIR/G)-11.334	(Hou, 2013)
TSS I	$119.62(R/G)^{6.0823}$	(Zhu et al., 2015)
TSS II	$49.257\exp(2.5806(B+NIR))$	(Liu, 2023)
TSS III	$26.191(NIR/B)^2$+50.6(NIR/B)-5.1592	(Hou et al., 2018)
SD I	$11.5191(R/G)^{-4.0751}$	(Zhu et al., 2015)
SD II	-140.07(R/G)+165.6	(Fu et al., 2022)
SD III	$0.0876(R*G)^{-0.373}$	(Wen et al., 2023)

The R, G, B, NIR, VNIR1 and VNIR2 respectively denote the red, green, blue, near infrared, vegetation red edge 1 and vegetation red edge 2 band

Vine Copula joint probability distribution

Common Vine Copula functions

The Copula function is a tool used to connect the marginal distributions of multivariate random variables and construct multivariate distributions, exploring the relationships between random variables. However, as the dimensionality increases, the difficulty of solving joint distribution functions increases sharply, leading to the problem of "curse of dimensionality." Joe (1996) proposed the Vine Copula method, and Bedford and Cooke (2001) constructed the vine structure using Pair theory. This method converts a traditional m-dimensional Copula function into m(m-1)/2 bivariate Copula functions. Each edge corresponds to a Pair-Copula structure, forming a tree structure with univariate marginal distributions as nodes and bivariate Copula joint distributions as edges. This significantly reduces the difficulty of solving high-dimensional joint distribution functions and helps to analyze the internal correlation features of high-dimensional variables.

Among the various Copula functions, the Archimedean Copula function has a simple structure and is computationally efficient. It can construct a wide variety of multivariate joint distribution functions with strong adaptability, meeting the application requirements of most fields and holding an important position in practical applications. The elliptical Copula function, which originates from the elliptical distribution, is a commonly used family of Copula functions. It can fit the distribution of multivariate random variables and non-normal structures well. Common elliptical Copula functions include the Normal Copula and t-Copula functions. The Normal Copula cannot describe tail dependence, while the t-Copula can effectively describe symmetric tail dependence (Nguyen and Jayakumar, 2018; Qian et al., 2020). For non-tail dependence issues, Cech (2006) proposed the rotated Copula function, which involves rotating transformations of Joe, Gumbel, and Clayton, such as SurJoe. This study selects the Copula functions as presented in *Table 2*. The θ is the interrelationship between variables; the ϕ and T denote the distribution function; the u and v denote the variables.

http://www.aloki.hu ● ISSN 1589 1623 (Print) ● ISSN 1785 0037 (Online)
DOI: http://dx.doi.org/10.15666/aeer/2305_90759099

Table 2. *Parameters of the Copula function*

Typology	Formality
Gumbel	$\exp\{-[(-\ln u_1)^{\theta}+(-\ln u_2)^{\theta}]^{1/\theta}\},\theta\in[1,\infty)$
Frank	$-\ln\left[1+\left(e^{-\theta u_1}-1\right)\left(e^{-\theta u_2}-1\right)/\left(e^{-\theta}-1\right)\right]/\theta,\theta\in R$
Clayton	$\left(u_1^{-\theta}+u_2^{-\theta}-1\right)^{-1/\theta},\theta\in(0,\infty)$
t-Copula	$T_{\rho,\nu}\left[T_{\nu}^{-1}(u_1),\cdots,T_{\nu}^{-1}(u_n)\right]$
AMH	$uv/[1-\theta(1-u)(1-v)],\theta\in[-1,\infty)$
Tawn	$\exp\left\{\ln\left(u^{1-\theta_1}\right)+\ln\left(v^{1-\theta_2}\right)-\left[\left(-\theta_1\ln(u)\right)^{\theta_3}+\left(-\theta_2\ln(v)\right)^{\theta_3}\right]^{1/\theta_3}\right\},\theta_1,\theta_2\in[0,1],\theta_3\in[1,\infty)$
FGM	$uv[1+\theta(1-u)(1-v)],\theta\in[-1,1]$
Plackett	$\left[1+(\theta-1)(u+v)-\sqrt{[1+(\theta-1)(u+v)]^2-4\theta(\theta-1)uv}\right]/2(\theta-1),\theta\in(0,\infty)$
Joe	$1-[(1-u)^{\theta}+(1-v)^{\theta}-(1-u)^{\theta}(1-v)^{\theta}]^{1/\theta},\theta\in(1,\infty)$
Independence	uv
SurClayton	$u_1+u_2-1+\left((1-u_1)^{-\theta}+(1-u_2)^{-\theta}-1\right)^{-1/\theta},\theta\in(0,\infty)$
SurGumbel	$u_1+u_2-1+\exp\{-[(-\ln(1-u_1))^{\theta}+(-\ln(1-u_2))^{\theta}]^{1/\theta}\},\theta\in[1,\infty)$
SurJoe	$u_1+u_2-1+\left(u_1^{\theta}+u_2^{\theta}-u_1^{\theta}\cdot u_2^{\theta}\right)^{1/\theta},\theta\in(1,\infty)$

Establishing marginal distributions

The construction of marginal distributions in traditional Copula functions relies on the Copula family of distributions, where it is necessary to assume that the sequence $\{x_n\}$ follows a specific distribution. In contrast, the Kernel Density Estimation method for solving marginal distributions does not limit itself to any distributional assumptions and can maximize the fit to the random variable distribution, using a kernel function to derive the probability density function (Zhang and Jiang, 2019; Heredia-Zavoni and Montes-Iturrizaga, 2022). Based on the simulation results from the water quality parameter inversion model, a simulated sequence of water body parameter indicators $\{x_n|n=1,2,\cdots,N\}$ is obtained, where N is the number of simulated sequences. For any sample value x_m in the sequence $\{x_n\}$, if the number of values less than x_m in the sequence $\{x_n\}$ is N_m, the cumulative frequency corresponding to x_m can be expressed by *Eq.4*. For water quality parameters, the parameter variable is $\{x_n\}$, and if the given control limit for a specific eutrophication level of the water body is x_k, then *Eq.5* can represent the risk of exceeding the pollution threshold for that pollutant.

$$\hat{f}_h(x)=[\sum_{i=1}^{n} K((x-x_i)/h)]/hn, \quad \text{(Eq.3)}$$

$$P(x_m)=P(x_i\leq x_m)=N_m/N, \quad \text{(Eq.4)}$$

$$P_k=P(x_i>x_k), \quad \text{(Eq.5)}$$

where K is the kernel function, and h is the bandwidth ($h>0$); in *Eq.4*, x_i represents a specific water quality monitoring indicator, and $P(x_m)$ is the frequency function for the event $x_i\leq x_m$; in *Eq.5*, x_i represents a specific water quality monitoring indicator, and P_k is the frequency function for the event $x_i>x_k$.

http://www.aloki.hu ● ISSN 1589 1623 (Print) ● ISSN 1785 0037 (Online)
DOI: http://dx.doi.org/10.15666/aeer/2305_90759099

By combining *Eqs.3,4, and 5*, the overall approximate distribution is determined using the kernel density estimation function based on the frequency of all sample values in the simulated sequence $\{x_n\}$, and the marginal distributions for each parameter indicator are constructed.

Selection of Vine Copula functions

To analyze the joint risk probability of water body eutrophication indicators, the most suitable Copula function is selected based on the squared Euclidean distance under the two-dimensional random variable state, and the optimal Copula joint probability distribution model is established. However, in the high-dimensional Vine structure, increasing the number of variables rapidly increases the complexity of the tree structure. When decomposing the high-dimensional structure, the Akaike Information Criterion (AIC) (Akaike, 1974) for each edge in the tree structure is usually used to determine the optimal Copula function. Parameters are then estimated using the maximum likelihood estimation method (Shih and Louis, 1995), and the connection order of the root node is determined. The optimal Vine structure is derived by calculating the total AIC of the tree structure. As shown in *Eq.6*:

$$AIC=2Q-2\ln(L), \quad \text{(Eq.6)}$$

where Q and L respectively denote the number of model parameters and logarithm of the likelihood function of the model.

Joint probability distribution

Eutrophication of water bodies is a composite indicator that leads to an increase in aquatic plants, severely affecting water ecological functions and water quality. Therefore, it is typically evaluated using multiple water quality parameters. This study uses Vine Copula theory to establish the joint probability distribution between various water quality parameter indicators, thus enabling a comprehensive analysis of the eutrophication risk of water bodies (Hochrainer-Stigler et al., 2018).

Let $X(x_1,\cdots x_d)$ represent the indicator sequence of water body eutrophication-related parameters. According to Sklar's theorem (Sklar, 1959), the multivariate joint distribution function can be expressed as *Eq. 7*:

$$F_{1,2,\cdots,d}(x_1,x_2,\cdots,x_d)=C[F_1(x_1),F_2(x_2),\cdots,F_d(x_d)]=C(u_1,u_2,\cdots,u_d), \quad \text{(Eq.7)}$$

where $F_1(x_1),F_2(x_2),\cdots,F_d(x_d)$ represent the marginal cumulative distribution functions, and $F_{1,2,\cdots,d}(x_1,x_2,\cdots,x_d)$ represents the joint probability distribution function. Based on conditional probability, the probability density function of the two-dimensional random variable is shown in *Eq.8*:

$$f(x_i,x_j)=C_{ij}\left(F_i(x_i),F_j(x_j)\right)f(x_i)f(x_j), \quad \text{(Eq.8)}$$

where $C_{ij}\left(F_i(x_i),F_j(x_j)\right)$ is the bivariate Copula density function of x_i and x_j, and the conditional probability density of x_i is shown in *Eq.9*:

http://www.aloki.hu ● ISSN 1589 1623 (Print) ● ISSN 1785 0037 (Online)
DOI: http://dx.doi.org/10.15666/aeer/2305_90759099

$$f(x_i|x_j)=C_{ij}\left(F_i(x_i),F_j(x_j)\right)f(x_i). \quad \text{(Eq.9)}$$

Taking the three-dimensional random variable distribution as an example, *Eq.9* gives:

$$f(x_1|x_2,x_3)=C_{13|2}\{F(x_1|x_2),F(x_3|x_2)\}\cdot f(x_1|x_2), \quad \text{(Eq.10)}$$

$$f(x_1|x_2)=C_{12}\{F_1(x_1),F_2(x_2)\}\cdot f_1(x_1). \quad \text{(Eq.11)}$$

Substituting *Eq.11* into *Eq.10* yields *Eq.12*:

$$f(x_1|x_2,x_3)=C_{13|2}\{F(x_1|x_2),F(x_3|x_2)\}\cdot f(x_1|x_2)\cdot C_{12}\{F_1(x_1),F_2(x_2)\}\cdot f_1(x_1). \quad \text{(Eq.12)}$$

The decomposed three-dimensional probability density function is given in *Eq.13*:

$$f(x_1,x_2,x_3)=f_3(x_3)\cdot C_{23}\{F_2(x_2),F_3(x_3)\}\cdot f_2(x_2)\cdot C_{13|2}\{F(x_1|x_2),F(x_3|x_2)\}\cdot f(x_1|x_2)\cdot C_{12}\{F_1(x_1),F_2(x_2)\}\cdot f_1(x_1) \quad \text{(Eq.13)}$$

Principle of geographic detector

Geographic Detector is mainly used to explore spatial heterogeneity and analyze the relevant driving factors by combining continuous and categorical data (Wang and Xu, 2017). It includes factor detectors, interaction detectors, risk detectors, and ecological detectors. The main advantage of Geographic Detector is its ability to detect the interaction between pairs of factors and their effect on the dependent variable. Through interaction detection, it examines the explanatory power of pairs of factors on the dependent variable, i.e., the interaction relationship between independent and dependent variables. In this study, Chl-a, TSS, and SD are selected as independent variables, and the factor interaction detector is used to investigate the water body's Comprehensive Trophic Level Index.

Results and discussion

Water quality parameter inversion

Current research on remote sensing monitoring water quality models is mostly based on the inherent optical characteristics of water bodies. Studies have shown that Chl-a exhibits distinct spectral features (Niu et al., 2024), and the inversion using remote sensing technology has high accuracy. Additionally, Chl-a concentration is an important parameter for assessing eutrophication in inland water bodies. In inland water bodies, SD generally shows a certain negative correlation with Chl-a and TSS. However, the spectral characteristics of non-optically active substances such as TN and TP are difficult to obtain, and the spectral response mechanisms are not clear. Therefore, Chl-a does not necessarily have a stable relationship with TP, TN, and other substances.

The Kendall correlation coefficient does not rely on linear assumptions, is more robust to outliers, and has stronger general applicability. In this study, the Kendall correlation coefficient was used to select three combinations with better correlation, resulting in relatively accurate inversion models. As shown in *Fig. 4*, the combinations (Chl-a III,

http://www.aloki.hu ● ISSN 1589 1623 (Print) ● ISSN 1785 0037 (Online)
DOI: http://dx.doi.org/10.15666/aeer/2305_90759099

TSS II, SD III) in 2017 were relatively reasonable, with Kendall correlation coefficients of 0.658 and -0.2388 for (Chl-a III, TSS II) and (TSS II, SD III), respectively. Similarly, in 2018, the combinations (Chl-a I, TSS II, SD III), (Chl-a I, TSS II), and (TSS II, SD III) had Kendall correlation coefficients of 0.9189 and -0.3805, respectively. In 2019, the combinations (Chl-a III, TSS II, SD III), (Chl-a III, TSS II), and (TSS II, SD III) had Kendall correlation coefficients of 0.5742 and -0.3275, respectively.

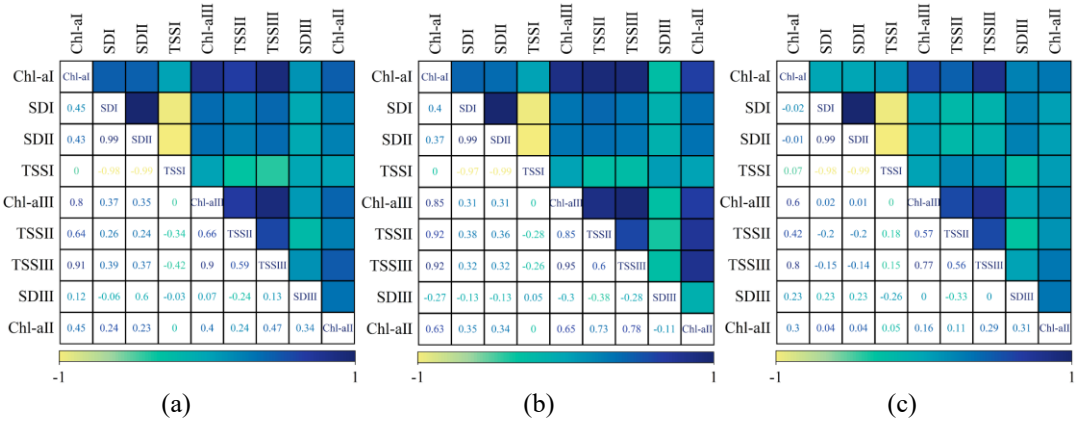

Figure 4. *Kendall correlation for different models. In inland water bodies, the overall SD exhibits a certain negative correlation with both Chl-a and TSS. By using the Kendall correlation coefficient, three combinations with better correlations are selected, leading to the development of relatively accurate inversion models. (a) Correlation of the inversion model in 2017. (b) Correlation of the inversion model in 2018. (c) Correlation of the inversion model in 2019*

Chl-a is an important parameter for evaluating the eutrophication of inland waters (García-Nieto et al., 2022; Saravani et al., 2025), serving as an objective biological indicator reflecting the nutritional status of water bodies. As shown in *Figs. 5-7*. From an overall distribution perspective, the Chl-a concentration is relatively high in the middle section of North Lake, the western and middle sections of Leijia Ditch, the western section of Yongchun River, and the southern section of Fuyu River, significantly higher than in reservoirs, with the highest value reaching 55.13 μg/L. According to China's nutritional state grading standards for corresponding indicators, a Chl-a concentration greater than 26 μg/L is considered eutrophic, indicating that eutrophication is severe in the four typical water bodies mentioned above.

In terms of TSS content, TSS can bring suspended particles and other insoluble organic and inorganic substances, affecting water quality. In the middle section of North Lake, the middle section of Leijia Ditch, the western section of Yongchun River, and the southern section of Fuyu River, TSS content shows a significant difference compared to other water bodies, fluctuating around 200 mg/L, with the maximum value reaching 218.35 mg/L. SD is closely related to TSS content and composition, showing a certain negative correlation. Lower transparency leads to water quality deterioration, thus damaging the water body's functions and disrupting the ecological balance.

From a temporal perspective, following the promulgation of the "Water Pollution Prevention and Control Action Plan" (also known as "Water Ten Measures") in 2015, which strengthened water environmental governance, between 2017 and 2019, the Chl-a concentration in typical water bodies decreased from (27.13, 42.60) μg/L to (26.07, 38.07) μg/L, with a change of 10.63%; TSS content decreased from (100.03, 208.20)

http://www.aloki.hu ● ISSN 1589 1623 (Print) ● ISSN 1785 0037 (Online)
DOI: http://dx.doi.org/10.15666/aeer/2305_90759099

mg/L to (84.32, 198.27) mg/L, a year-on-year decrease of 4.77%; SD, in addition to being closely related to TSS content, is also influenced by the composition of suspended solids, so changes in water transparency showed slight fluctuations, with an overall change of 9.71%.

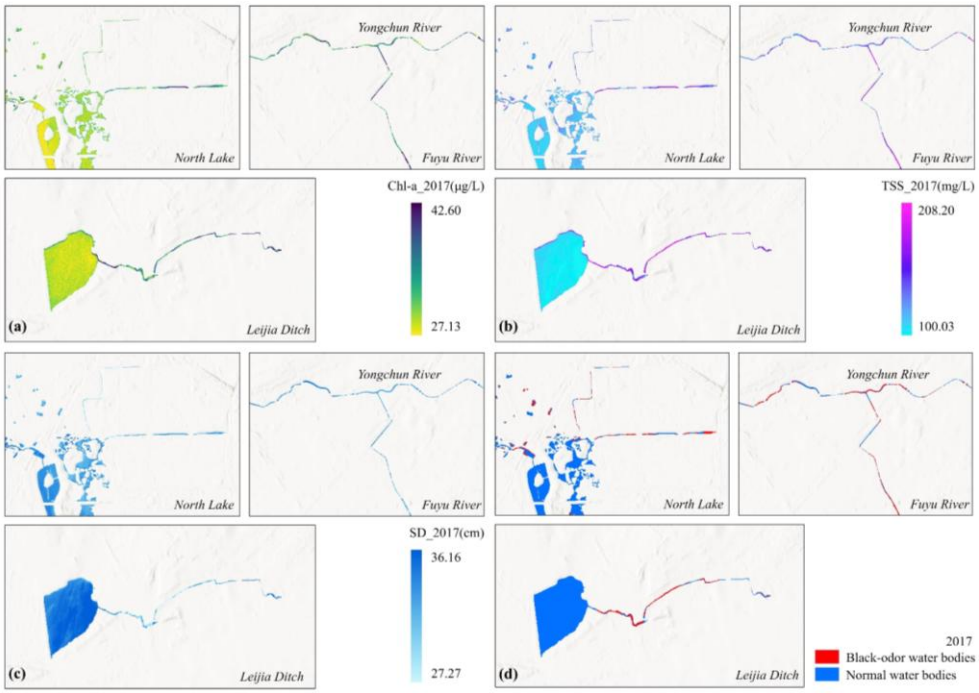

Figure 5. *Inversion of water quality parameters and identification of black-odor water bodies in 2017. The Chl-a, TSS, and SD denote chlorophyll-a, total suspended solids, and secchi depth, respectively. The SEaTH algorithm is used to construct a four-dimensional feature space, which is then combined with Support Vector Machine for the identification of black and odorous water bodies. Subsequently, inversion models are applied to retrieve water quality parameters such as Chl-a, TSS, and SD. (a) The results of Chl-a inversion. (b) The results of TSS inversion. (c) The results of SD inversion. (d) The results of black-odor water bodies identification*

According to the SEaTH algorithm, feature importance is identified to construct a multidimensional feature space. By combining optimal support vectors and hyperplanes, black-odor water information is extracted from the typical water bodies of North Lake, Leijia Ditch, Yongchun River, and Fuyu River. Generally, the BOI index for black-odor water bodies ranges between (-0.05, 0.06) (Yao et al., 2019). Based on the preliminary identification results and combined with 88 feature values such as spectral Mean, Variance, Contrast, Correlation, Entropy, Homogeneity, Dissimilarity, and Second Moment, the Second Moment, Contrast, and Correlation were ultimately selected to construct four-dimensional feature spaces for the years 2017 (NIR Con, R Sec, VNIR2 Sec, VNIR4 Sec), 2018 (VNIR3 Sec, VNIR4 Sec, R Sec, R Cor), and 2019 (VNIR3 Sec, VNIR4 Sec, NIR Sec, R Sec). Support Vector Machine was then used for black-odor water body identification.

http://www.aloki.hu ● ISSN 1589 1623 (Print) ● ISSN 1785 0037 (Online)
DOI: http://dx.doi.org/10.15666/aeer/2305_90759099

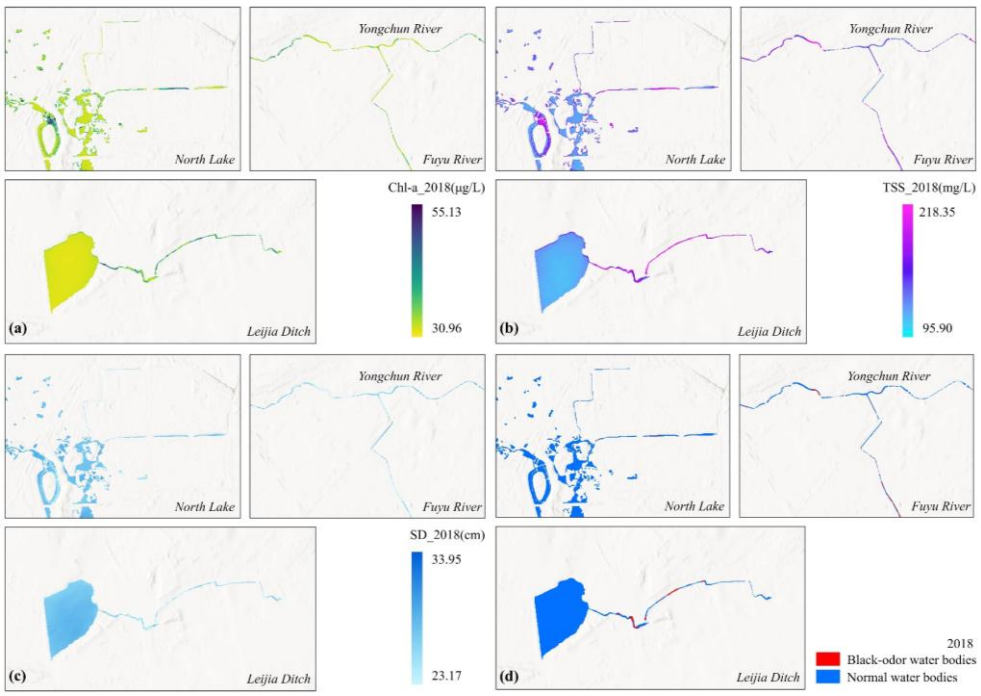

Figure 6. *Inversion of water quality parameters and identification of black-odor water bodies in 2018. The Chl-a, TSS, and SD denote chlorophyll-a, total suspended solids, and secchi depth, respectively. (a) The results of Chl-a inversion. (b) The results of TSS inversion. (c) The results of SD inversion. (d) The results of black-odor water bodies identification*

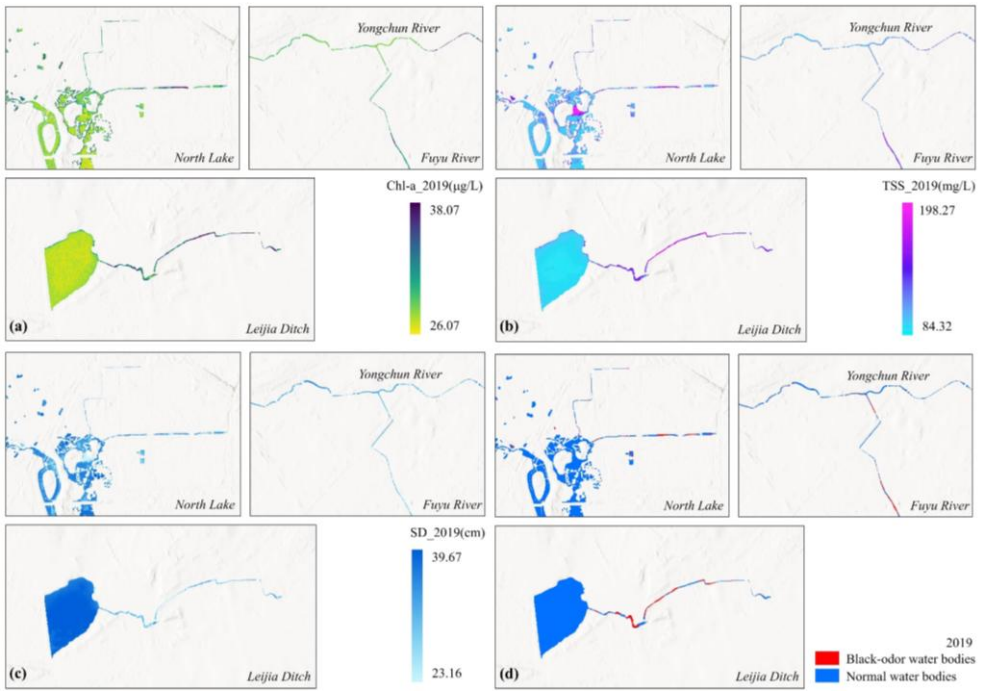

Figure 7. *Inversion of water quality parameters and identification of black-odor water bodies in 2019. The Chl-a, TSS, and SD denote chlorophyll-a, total suspended solids, and secchi depth, respectively. (a) The results of Chl-a inversion. (b) The results of TSS inversion. (c) The results of SD in-version. (d) The results of black-odor water bodies identification*

http://www.aloki.hu ● ISSN 1589 1623 (Print) ● ISSN 1785 0037 (Online)
DOI: http://dx.doi.org/10.15666/aeer/2305_90759099

Two-dimensional joint distribution

The optimal combination model, selected using Kendall's correlation coefficient, is employed to invert the parameter indicator sequences, thereby obtaining the empirical frequency distributions of the individual parameter indicators. The kernel density estimation function is not confined to any predefined probability density function form. It estimates the probability density of a data point by performing a weighted average of kernel functions around each data point, offering high computational efficiency and structural flexibility. Based on the empirical frequency distributions of the nine parameter indicators, the joint distribution model is solved using kernel density estimation in combination with the Copula function to obtain the univariate distribution.

Using the one-dimensional distribution of eutrophication parameters to construct the two-dimensional joint distribution, as shown in *Table 3*, a total of 9 combinations were considered between 2017 and 2019, including (Chl-a, TSS), (Chl-a, SD), and (TSS, SD). The goodness of fit of each combination was evaluated using the squared Euclidean distance, and the most suitable Copula function was determined for constructing the optimal joint distribution model for each combination. For most combinations, the squared Euclidean distance of different Copula functions tended to approach zero. The smaller the value, the better the fit, indicating the most suitable Copula function for that combination.

Table 3. *Evaluation of fitting based on Squared Euclidean Distance*

	2017			**2018**			**2019**		
	(Chl-a, TSS)	(Chl-a, SD)	(TSS, SD)	(Chl-a, TSS)	(Chl-a, SD)	(TSS, SD)	(Chl-a, TSS)	(Chl-a, SD)	(TSS, SD)
Clayton	0.4610	0.1523	0.3098	0.0229	0.2586	0.4664	0.3337	0.3791	0.9355
Frank	0.1317	0.1271	0.0384	0.0144	0.0740	0.0917	0.0487	0.4105	0.1857
Gaussian	0.1459	0.1245	0.0480	0.0205	0.1041	0.1230	0.0690	0.4190	0.2503
Gumbel	0.0867	0.1070	0.3098	0.0155	0.2586	0.4664	0.0502	0.4691	0.9355
t-Copula	0.1715	1.8332	3.0432	0.0790	1.7744	2.4216	0.1644	2.9094	5.5046

The Chl-a, TSS, and SD denote chlorophyll-a, total suspended solids, and Secchi depth, respectively

For the (Chl-a, TSS) combination in 2018, the smallest squared Euclidean distance among the Copula functions was 0.0144, indicating that the Frank Copula function provided the best fit for this combination. In contrast, for the (TSS, SD) combination in 2019, the smallest squared Euclidean distance for the t-Copula function was as high as 5.5046, indicating a more dispersed data distribution and poor goodness of fit under the t-Copula function.

Following the principle of the smallest squared Euclidean distance, the most suitable Copula function for each of the 9 combinations was selected. As shown in *Fig. 8*, the most appropriate Copula functions for the (Chl-a, SD) combination from 2017 to 2019 were Gumbel Copula, Frank Copula, and Clayton Copula, respectively; for the (Chl-a, TSS) combination, they were Gumbel Copula, Frank Copula, and Frank Copula; and for the (TSS, SD) combination, Frank Copula was selected for all three years. The optimal joint distribution models for each combination were then calculated based on the empirical theoretical joint frequency values, with data concentrated near the line, demonstrating a good fit.

http://www.aloki.hu ● ISSN 1589 1623 (Print) ● ISSN 1785 0037 (Online)
DOI: http://dx.doi.org/10.15666/aeer/2305_90759099

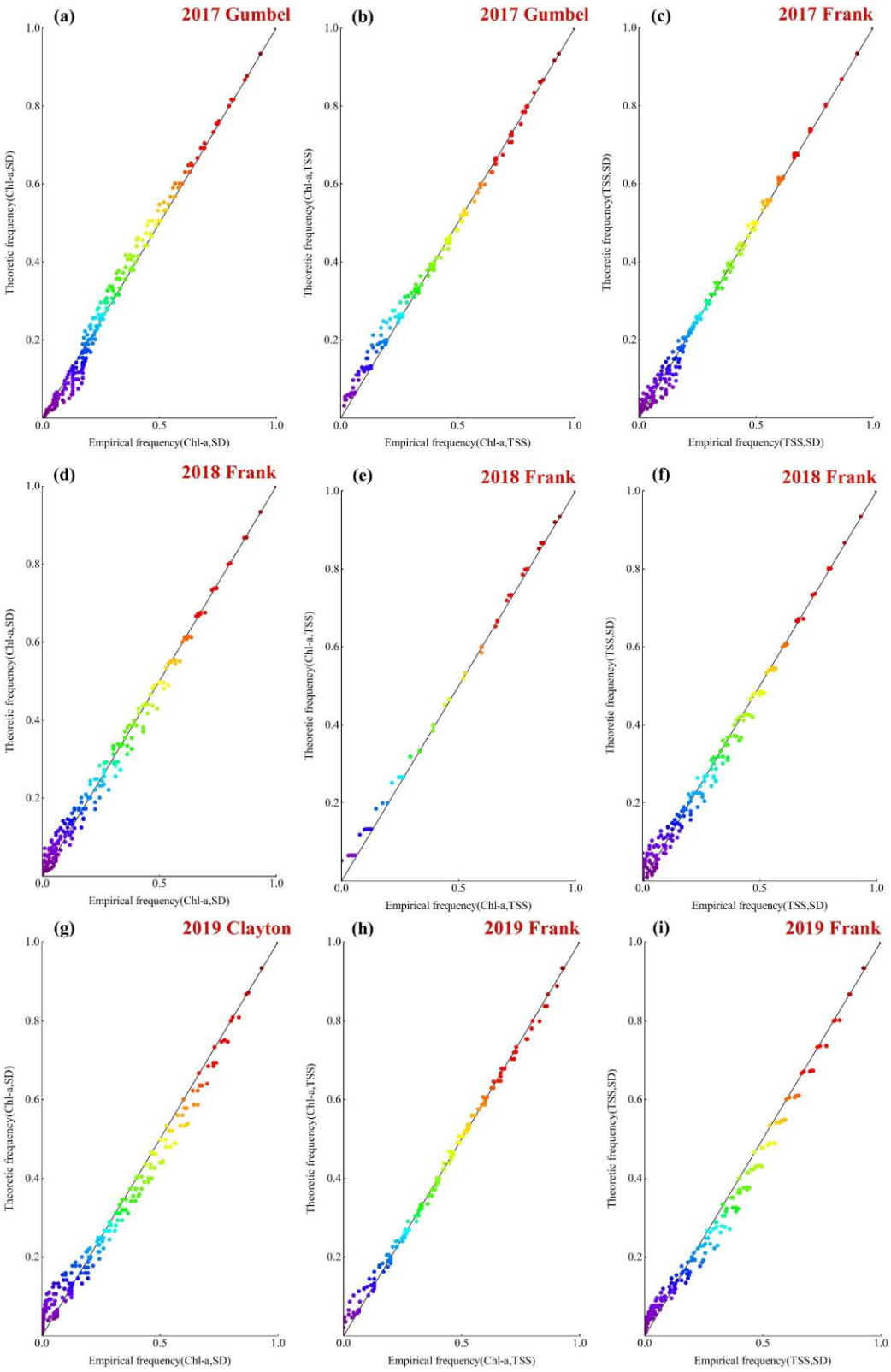

Figure 8. *Fitting results of the optimal Copula function based on empirical and theoretical frequencies. The most suitable Copula function for each combination is determined using the squared Euclidean distance, and the optimal joint distribution model is constructed. A smaller squared Euclidean distance indicates a better fitting performance of the model*

http://www.aloki.hu ● ISSN 1589 1623 (Print) ● ISSN 1785 0037 (Online)
DOI: http://dx.doi.org/10.15666/aeer/2305_90759099

As shown in *Table 4*, to facilitate the analysis of the joint risk probability model, the parameter indicator sequences of the typical water bodies were divided into five levels based on their concentrations. As shown in *Table 5* and *Fig. 9*, as the levels of each parameter indicator increased, the risk probability of eutrophication progressively increased. In 2017, when both TSS and SD were at Level I, the joint risk probability of the two was only 0.36%, indicating that the impact on water quality was minimal under this condition. When both Chl-a and TSS were at Level I, the joint risk probability increased to 31.31%, suggesting that this combination had a greater impact on water quality at Level I. When SD remained at the same level, the eutrophication risk probability increased progressively as the levels of TSS and Chl-a increased. In comparison, TSS had a more significant effect on the increase in risk probability. Notably, when SD was at Level III, an increase in TSS from Level I to Level IV led to a 49.28% increase in risk probability, whereas Chl-a only caused a 44.55% increase in risk probability. However, there was a special case: when SD was at Level V, the increase in risk probability caused by Chl-a (62%) was higher than that caused by TSS (60%).

Table 4. *Risk level thresholds of water quality indicators*

Water quality indicators	**Risk level**				
	I	II	III	IV	V
Chl-a (μg/L)	32.69	37.95	43.21	48.47	53.73
TSS (mg/L)	137.11	170.65	204.18	237.72	271.26
SD (cm)	36.45	34.06	31.67	29.28	26.89

The Chl-a, TSS, and SD denote chlorophyll-a, total suspended solids, and secchi depth, respectively

Table 5. *Two-Dimensional joint risk probability (%) under different combination methods*

	2017(Chl-a)					**2018(Chl-a)**					**2019(Chl-a)**			
	I	II	III	IV	V	I	II	III	IV	V	I	II	III	IV
I(SD)	0.89	1.69	1.92	1.97	2	0.00	0.00	0.00	0.00	0.00	1.32	1.88	1.92	2
II(SD)	8.25	16.73	19.12	19.73	20	0.00	0.00	0.00	0.00	0.00	11.88	16.92	17.28	18
III(SD)	29.45	60.64	70.33	72.87	74	0.00	0.68	1.35	2.45	3.6	23.76	33.84	34.56	36
IV(SD)	33.64	69.98	81.54	84.62	86	0.00	37.82	56.89	76.32	90.06	52.8	75.2	76.8	80
V(SD)	38	80	94	98	100	0.00	0.00	0.00	0.00	0.00	60.72	86.48	88.32	92
	2017(Chl-a)					**2018(Chl-a)**					**2019(Chl-a)**			
	I	II	III	IV	V	I	II	III	IV	V	I	II	III	IV
I(TSS)	31.31	39.8	40	40	40	0.00	24	24	24	24	57.81	67.23	67.52	68
II(TSS)	37.95	78.25	85.68	85.99	86	0.00	41.88	47.99	48	48	65.33	89.78	91.25	94
III(TSS)	38	79.96	93.46	95.84	96	0.00	42	61.88	67.99	68	65.8	92.65	94.46	98
IV(TSS)	38	80	93.93	97.47	98	0.00	42	62	81.95	89.9	66	94	96	100
V(TSS)	38	80	94	98	100	0.00	42	62	81.98	91.75	0.00	0.00	0.00	0.00
	2017(TSS)					**2018(TSS)**					**2019(TSS)**			
	I	II	III	IV	V	I	II	III	IV	V	I	II	III	IV
I(SD)	0.36	1.42	1.82	1.91	2	0.00	0.00	0.00	0.00	0.00	0.67	1.64	1.87	2
II(SD)	4.27	14.94	18.45	19.22	20	0.00	0.00	0.00	0.00	0.00	7.14	15.39	17.1	18
III(SD)	24.72	61.58	70.41	72.2	74	0.16	0.55	1.24	2.81	3.02	16.85	31.82	34.58	36
IV(SD)	31.33	72.74	82.19	84.09	86	20.57	43	62.4	84.08	86.06	50.02	74.25	78.08	80
V(SD)	40	86	96	98	100	0.00	0.00	0.00	0.00	0.00	60.67	86.08	90.02	92

The Chl-a, TSS, and SD denote chlorophyll-a, total suspended solids, and secchi depth, respectively

http://www.aloki.hu ● ISSN 1589 1623 (Print) ● ISSN 1785 0037 (Online)
DOI: http://dx.doi.org/10.15666/aeer/2305_90759099

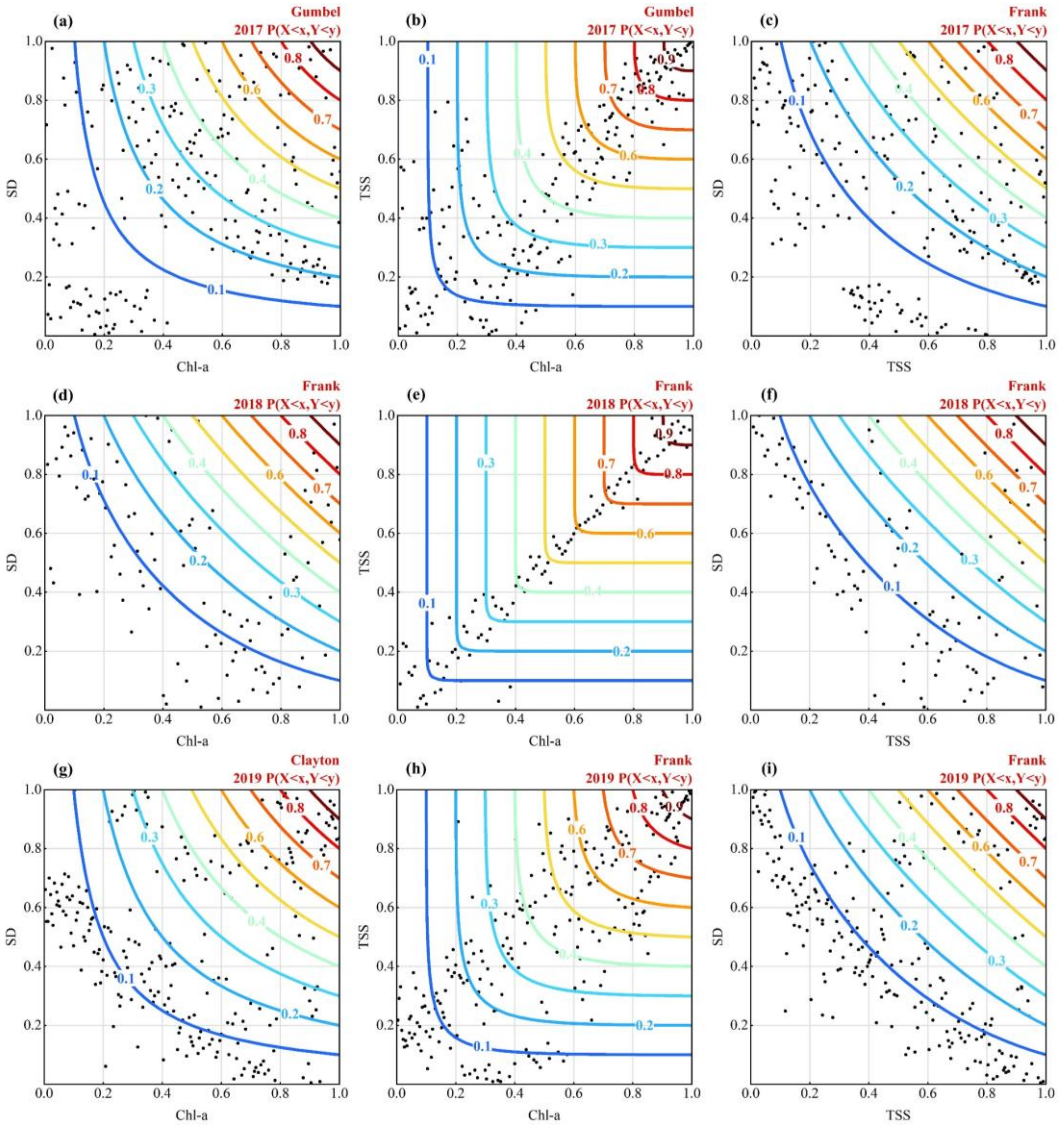

Figure 9. *Two-Dimensional joint probability distribution under different combination methods. The Chl-a, TSS, and SD denote chlorophyll-a, total suspended solids, and Secchi depth, respectively. The optimal Copula joint distribution model is selected to assess the eutrophication risk of black-odor water bodies*

In 2018, when both Chl-a and TSS were at Level V, and when Chl-a was at Level V and SD at Level IV, the maximum risk probabilities were 91.75% and 90.06%, respectively, indicating that these two combinations had a large impact on water quality. For the (TSS, SD) combination, the maximum risk probability was 86.06%, lower than 90.06%, suggesting that this combination had a smaller impact on water quality. Moreover, a positive correlation has been observed between Chl-a and TSS, whereas both Chl-a and TSS exert negative effects on SD (Mamun et al., 2024). With steady progress in water ecological governance, the risk probability in 2018 decreased compared to 2017. However, during activities such as dredging and water environment construction, some bottom sediments and garbage were piled along the shore without scientific and effective disposal, causing pollutants in leachate to be directly discharged into rivers during the rainy season. This was one of the reasons for the re-occurrence of black and foul-smelling

http://www.aloki.hu ● ISSN 1589 1623 (Print) ● ISSN 1785 0037 (Online)
DOI: http://dx.doi.org/10.15666/aeer/2305_90759099

water in typical water bodies in 2019. For the (Chl-a, SD) and (TSS, SD) combinations, the maximum risk probabilities increased from 90.06% and 86.06% in 2018 to 92% in 2019, indicating that the water quality was significantly affected.

Three-dimensional joint distribution

By comparing the AIC values, the goodness of fit for the Vine Copula model is evaluated. The smaller the AIC value, the better the fit. For each connecting edge (1: Chl-a, 2: TSS, 3: SD), the Copula function with the smallest AIC value is selected, and the optimal tree structure is determined based on the total AIC value. As shown in *Tables 6* and *7*, the optimal function for the year 2017 is determined.

Table 6. *Optimal Vine parameters and AIC values*

Tree	Edge	Copula	Parameters	AIC	Total AIC
T1	3,2	FGM	-1	-28.7284	-428.274
	2,1	Joe	4.032	-266.0578	
T2	3,1 | 2	t-Copula	0.5447,2.239	-133.4878	

Table 7. *AIC values of different Copula functions*

Copula	AIC	Copula	AIC
Gumbel	-85.1416	FGM	-71.8708
AMH	-108.0343	Tawn	-83.7825
t-Copula	-133.4878	Joe	-38.6676
Gaussian	-63.9137	SurJoe	-122.4092
Frank	-99.4009	SurClayton	-45.4097
Clayton	-125.2197	SurGumbel	-120.139
Independence	1455.6	Plackett	-105.5734

Based on the optimal Copula function models established for different years, the joint risk probabilities of water eutrophication were evaluated, as shown in *Table 8*. In 2017, when Chl-a was at level II, TSS at level IV, and SD at level V, the joint risk probability reached 44.41%. In 2018, when both Chl-a and TSS were at level V and SD was at level IV, the risk probability decreased to 34.96%. In 2019, when Chl-a was at level IV, TSS at level III, and SD at level V, the risk probability increased to 51.73%. These results suggest that the joint risk probabilities were relatively high under these conditions, indicating a considerable impact on water quality.

With the steady advancement of water ecological restoration efforts, the maximum risk probability in 2018 decreased to 34.96%, reflecting significant improvements in water ecological function restoration. However, despite these advancements, certain challenges remain. Specifically, industries such as raw material manufacturing and chemical production in urban areas, which are major sources of pollution, have not undergone timely restructuring or relocation. Additionally, industrial wastewater discharge has not been effectively managed through a long-term control mechanism. As a result, the risk probability increased to 51.73% in 2019, exacerbating the occurrence of blackening and foul odor phenomena in the water. To tackle eutrophication, a wide range of measures need to be implemented, such as the proper management of agricultural and industrial wastewater discharges, the enhanced monitoring and remediation of water

http://www.aloki.hu ● ISSN 1589 1623 (Print) ● ISSN 1785 0037 (Online)
DOI: http://dx.doi.org/10.15666/aeer/2305_90759099

bodies. These measures contribute to reducing nutrient inputs into water bodies and safeguarding the health of aquatic ecosystems (Qi et al., 2024). However, the most direct and effective method is sediment dredging, which has been successfully implemented in numerous cases, both domestically and internationally. For example, this technique has been applied in Lake Kasumigaura in Japan and Nanhu Lake in Changchun to control the release of endogenous nutrient substances (Murakami, 1984; Zhang, 2014; Mundahl, 2021; Wu, 2023).

Table 8. *Three-Dimensional joint risk probability (%) under different combination methods*

Joint risk probability		2017(TSS)					2018(TSS)					2019(TSS)			
		I	II	III	IV	V	I	II	III	IV	V	I	II	III	IV
I(SD)	I(Chl-a)	0.1	1.62	0.44	1.2	0.86	0.00	0.00	0.00	0.00	0.00	0.4	0.02	0.05	0.17
	II(Chl-a)	0.08	0.02	1.2	0.53	1.03	0.00	0.00	0.00	0.00	0.00	0.01	0.11	0.08	0.01
	III(Chl-a)	0.07	0.27	0.11	0.03	0.05	0.00	0.00	0.00	0.00	0.00	0.12	0.97	0.05	0.48
	IV(Chl-a)	0.35	0.1	0.63	1.25	0.19	0.00	0.00	0.00	0.00	0.00	0.26	0.15	0.18	0.41
	V(Chl-a)	0.00	0.53	2.49	2.41	0.62	0.00	0.00	0.00	0.00	0.00	0.00	0.00	0.00	0.00
II(SD)	I(Chl-a)	0.01	0.21	0.16	0.45	2.1	0.00	0.00	0.00	0.00	0.00	0.04	0.77	6.85	1.69
	II(Chl-a)	0.00	2.16	0.00	1.43	0.39	0.03	0.00	0.02	0.94	0.08	0.86	0.61	0.21	13.29
	III(Chl-a)	0.02	0.01	0.5	0.17	0.01	0.03	0.01	0.00	0.1	0.07	1.33	0.03	0.1	8.71
	IV(Chl-a)	0.36	0.7	0.3	0.86	2.44	0.12	0.01	0.22	1.92	0.01	5.63	0.28	0.71	0.15
	V(Chl-a)	0.03	0.42	3.89	0.99	0.15	0..01	0.22	0.08	1.45	0.07	0.00	0.00	0.00	0.00
III(SD)	I(Chl-a)	4.15	0.93	0.19	3.8	0.18	0.00	0.00	0.00	0.00	0.00	1.02	15.71	1.02	2.03
	II(Chl-a)	10.91	1.77	0.73	0.49	7.5	0.02	0.14	0.44	1.44	0.31	0.45	0.87	1.94	8.86
	III(Chl-a)	0.74	13.68	1.9	35.79	1.09	0.03	0.04	0.1	2.38	0.66	4.02	6.77	6.01	3.04
	IV(Chl-a)	2.31	0.92	2.68	1.77	0.27	0.05	0.00	0.01	0.35	5.22	0.03	7.7	0.12	1.53
	V(Chl-a)	8.17	5.66	4.24	20.85	3.85	0.11	0.23	0.92	0.37	0.73	0.00	0.00	0.00	0.00
IV(SD)	I(Chl-a)	0.36	7.05	0.83	5.98	0.15	0.00	0.00	0.00	0.00	0.00	4.69	8.62	2.06	1.81
	II(Chl-a)	4.81	2.7	6.74	2.86	9.93	0.5	0.13	9.31	21.64	15.97	1.91	12.65	8.95	8.8
	III(Chl-a)	3.37	3.91	0.01	9.7	1.28	3.17	4.27	5.88	1.11	27.18	0.17	4.87	9.89	9.01
	IV(Chl-a)	0.79	3.18	3.2	6.09	3.66	0.21	12.6	7.14	0.52	16.62	2.9	0.18	6.67	34.99
	V(Chl-a)	7.76	6.05	5.82	0.73	1.49	12.49	11.62	1.74	10.5	34.96	0.00	0.00	0.00	0.00
V(SD)	I(Chl-a)	4.79	23.14	1.53	5.12	3.04	0.00	0.00	0.00	0.00	0.00	8.06	17.45	5.09	5.01
	II(Chl-a)	1.81	8.99	13.69	44.41	21.46	0.00	0.00	0.00	0.00	0.00	17.7	2.65	6.62	0.3
	III(Chl-a)	14.86	23.97	0.05	26.57	5.62	0.00	0.00	0.00	0.00	0.00	8.8	16.48	0.1	39.78
	IV(Chl-a)	8.19	24.75	7.19	7.94	36.34	0.00	0.00	0.00	0.00	0.00	9.08	3.37	51.73	0.57
	V(Chl-a)	8.78	0.17	0.06	0.73	8.54	0.00	0.00	0.00	0.00	0.00	0.00	0.00	0.00	0.00

The Chl-a, TSS, and SD denote chlorophyll-a, total suspended solids, and secchi depth, respectively

From a temporal perspective, when Chl-a and SD are fixed at a certain risk level, the overall risk probability tends to increase with the elevation of TSS levels. For example, in 2019, when Chl-a was at level II and SD at level III, the risk probability increased from 0.45% to 8.86%. Given the complex composition of TSS and its close correlation with SD, the risk of eutrophication becomes more influenced by TSS composition when both TSS and SD reach higher levels (IV and V). As the concentrations of various components vary, the risk probability shows significant fluctuations. In general, an increase in the levels of Chl-a, TSS, and SD significantly raises the risk probability, thus impacting water quality. Further analysis of the interactions between factors is conducted using the Geographic Detector model.

http://www.aloki.hu ● ISSN 1589 1623 (Print) ● ISSN 1785 0037 (Online)
DOI: http://dx.doi.org/10.15666/aeer/2305_90759099

Geographical detector

This study employs the Comprehensive Trophic Level Index (TLI) in conjunction with interaction detection methods to conduct a correlation analysis of eutrophication risks in typical water bodies. The interaction detection approach allows for the identification of interactions between various factors, specifically evaluating the collective explanatory power of water quality parameters when jointly influencing the TLI. The calculation formulas for the TLI are given in *Eqs.14-16*:

$$TLI(Chl\text{-}a)=10(2.5+1.086\ln Chl\text{-}a) \quad \text{(Eq.14)}$$

$$TLI(SD)=10(5.118-1.94\ln SD) \quad \text{(Eq.15)}$$

$$TLI(\sum)=0.5921TLI(Chl\text{-}a)+0.4079TLI(SD) \quad \text{(Eq.16)}$$

As shown in *Table 9*, the detection results reveal, to some extent, the impact of interactions between water quality parameters on eutrophication. The interaction detection results predominantly indicate enhanced effects between pairs of factors of varying intensities; however, there are also instances of nonlinear enhancement. Additionally, the explanatory power of the interactions between factors on eutrophication is greater than the individual effects of each factor alone.

Table 9. *Interaction detection results of eutrophication risk impact factors from 2017 to 2019*

Interaction detection	**2017**			**2018**			**2019**		
	Chl-a	TSS	SD	Chl-a	TSS	SD	Chl-a	TSS	SD
Chl-a	0.5913			0.5251			0.1783		
TSS	0.8441	0.8100		0.8832	0.8702		0.7497	0.6281	
SD	0.9301	0.8802	0.5002	0.9499	0.9375	0.7305	0.9205	0.7982	0.7102

The Chl-a, TSS, and SD denote chlorophyll-a, total suspended solids, and secchi depth, respectively

From a temporal perspective, the explanatory power of individual factors such as Chl-a, TSS, and SD is relatively weak, with maximum values of 0.5913, 0.8702, and 0.7305, respectively. Compared to the effects of Chl-a and SD alone, TSS has a stronger impact on water body eutrophication. When these individual factors interact with the remaining factors, their explanatory power significantly increases to 0.9499, 0.9375, and 0.9499, demonstrating a substantial enhancement. However, when Chl-a and SD individually interact with TSS, the increase in explanatory power is relatively small, with an increase of 0.013 and 0.0673, respectively, in 2018. This can be attributed to the inherently weak explanatory power of Chl-a and SD on water body eutrophication, resulting in less noticeable improvement when they interact with TSS. Other studies have found that local land use, nutrient inputs, morphology, and hydrological dynamics can all exert significant influences on Chl-a, TSS, and SD in aquatic systems (Zimba and Gitelson, 2006; Ogashawara and Moreno-Madriñán, 2014; Pahlevan et al., 2014; Li et al., 2021). The increasing global temperature has been shown to degrade water quality, as demonstrated by studies conducted worldwide, including cases in China (Tian et al., 2024), Europe (Nõges et al., 2016; Bouraï et al., 2020), and the United States (Collins et al., 2019). The combined effects of these factors ultimately lead to the imbalance of aquatic ecosystems.

http://www.aloki.hu ● ISSN 1589 1623 (Print) ● ISSN 1785 0037 (Online)
DOI: http://dx.doi.org/10.15666/aeer/2305_90759099

Therefore, continuous and in-depth investigation of the key drivers of eutrophication is essential to provide valuable scientific support for aquatic ecosystem management and to effectively address environmental governance challenges.

Conclusion

a. Following the promulgation of the "Water Pollution Prevention and Control Action Plan" in 2015, the concentrations of Chl-a and TSS in typical water bodies from 2017 to 2019 demonstrated an initial increase, followed by a decline. In general, the reduction in Chl-a and TSS levels has contributed to mitigating the extent of eutrophication in the water bodies, thereby facilitating the improvement of the aquatic ecological environment.
b. By evaluating the goodness of fit, the optimal Vine Copula functions were selected. For the period of 2017, the best-fitting functions for the (Chl-a, TSS), (Chl-a, SD), and (TSS, SD) combinations were Gumbel, Gumbel, and Frank, respectively. In 2018, Frank was identified as the best-fitting function for all combinations. In 2019, the best-fitting functions for the combinations were Frank, Clayton, and Frank, respectively. For the (Chl-a, TSS, SD) combination, the optimal fitting functions for the years 2017-2019 were t-Copula, Gaussian, and Gumbel, respectively.
c. In the optimal Vine Copula function model, the risk probabilities for different combinations were computed. From 2017 to 2019, the highest risk probability exhibited an initial decrease followed by an increase. In 2019, the maximum risk probabilities for the (Chl-a, SD) and (TSS, SD) combinations were higher compared to 2018. When the SD level remained fixed, the increase in eutrophication risk was more significantly influenced by the elevation of Chl-a and TSS levels, with the composition and concentration of TSS also exerting a substantial impact on water quality.
d. Based on the results from the Geographical Detector, TSS demonstrated a strong explanatory power for eutrophication, which aligns with the findings from the Vine Copula model. In contrast, Chl-a and SD exhibited weaker explanatory power, and their interaction with TSS did not result in a significant enhancement of explanatory strength.

Overall, water eutrophication and degradation of water quality are not solely attributable to a single water quality parameter, but rather result from the interplay of multiple factors. These processes are intricately linked to issues such as inadequate urban planning and mismatched infrastructure (Wang et al., 2024; Zill et al., 2024; Vasilakou et al., 2025). Moving forward, the incorporation of a broader range of Vine Copula functions, along with the integration of additional evaluation indicators and an increase in the dimensionality of the model, would serve to enhance the objectivity and precision of eutrophication risk assessments. This approach is crucial for advancing water ecological restoration and improving the accuracy of environmental management strategies.

Acknowledgments. This research was funded by Foundation of Jilin Provincial Science & Technology Department (Grant No. YDZJ202201ZYTS499).

http://www.aloki.hu ● ISSN 1589 1623 (Print) ● ISSN 1785 0037 (Online)
DOI: http://dx.doi.org/10.15666/aeer/2305_90759099

REFERENCES

[1] Akaike, H. (1974): A new look at the statistical model identification. – IEEE transactions on automatic control 19(6): 716-723. https://doi.org/10.1109/TAC.1974.11007051.
[2] Azevedo, L. B., van Zelm, R., Leuven, R. S. E. W., Hendriks, A. J., Huijbregts, M. A. J. (2015): Combined ecological risks of nitrogen and phosphorus in European freshwaters. – Environmental Pollution 200: 85-92. https://doi.org/10.1016/j.envpol.2015.02.011.
[3] Barzegar, R., Aalami, M. T., Adamowski, J. (2020): Short-term water quality variable prediction using a hybrid CNN–LSTM deep learning model. – Stoch Environ Res Risk Assess. 34: 415-433. https://doi.org/10.1007/s00477-020-01776-2.
[4] Bedford, T., Cooke, R. M. (2001): Probability density decomposition for conditionally dependent random variables modeled by vines. – Annals of Mathematics and Artificial Intelligence 32(1/2/3/4): 245-268. https://doi.org/10.1023/A:1016725902970.
[5] Bhatti, M. I., Do, H. Q. (2019): Recent development in copula and its applications to the energy, forestry and environmental sciences. – International Journal of Hydrogen Energy 44(36): 19453-19473. https://doi.org/10.1016/j.ijhydene.2019.06.015.
[6] Biggs, B. J. F. (2000): Eutrophication of streams and rivers: dissolved nutrient-chlorophyll relationships for benthic algae. – Journal of the North American Benthological Society 19(1): 17-31.
[7] Bouraï, L., Logez, M., Laplace-Treyture, C., Argillier, C. (2020): How do eutrophication and temperature interact to shape the community structures of phytoplankton and fish in lakes? – Water 12: 779.
[8] Brito, I., Gonçalves, A. M., Pedra, A. (2024): Risk assessment for the surface water quality evaluation of a hydrological basin. – Stoch Environ Res Risk Assess. 38: 4527-4553. https://doi.org/10.1007/s00477-024-02817-w.
[9] Cantet, P., Arnaud, P. (2014): Extreme rainfall analysis by a stochastic model: impact of the copula choice on the sub-daily rainfall generation. – Stoch Environ Res Risk Assess. 28: 1479-1492. https://doi.org/10.1007/s00477-014-0852-0.
[10] Carstens, D., Amer, R. (2019): Spatio-temporal analysis of urban changes and surface water quality. – Journal of Hydrology 569: 720-734. https://doi.org/10.1016/j.jhydrol.2018.12.033.
[11] Cech, C. (2006): Copula-based top-down approaches in financial risk aggregation. – Available at SSRN 953888.
[12] Cheng, X., Xu, J., Li, Y., Zhang, Y., Zhu, Y., Cai, X., Lyu, H. (2024): Discrimination method of unmanned aerial vehicle hyperspectral for the types of pollution sources of black-odor rivers in cities. – National Remote Sensing Bulletin 28(8): 1914-1926.
[13] Collins, S. M., Yuan, S., Tan, P. N., Oliver, S. K., Lapierre, J. F., Cheruvelil, K. S., Fergus, C. E., Skaff, N. K., Stachelek, J., Wagner, T., Soranno, P. A. (2019): Winter precipitation and summer temperature predict lake water quality at macroscales. – Water Resour. Res. 55: 2708-2721.
[14] Czado, C., Nagler, T. (2022): Vine copula based modeling. – Annual Review of Statistics and Its Application 9(1): 453-477. https://doi.org/10.1146/annurev-statistics-040220-101153.
[15] Dall'Olmo, D., Gitelson, A. A. (2005): Effect of bio-optical parameter variability on the remote estimation of chlorophyll-a concentration in turbid productive waters: Experimental results. – Applied Optics 44(3): 412-422.
[16] Fu, L., Guo, W., Song, K., Liu, G. (2022): Remote Sensing Identification of Black and Odorous Water Bodies in Changchun City in 2020. – Wetland Science 20(4): 537-547.
[17] García-Nieto, P. J., García-Gonzalo, E., Alonso Fernández, J. R., Díaz Muñiz, C. (2022): Modeling eutrophication risks in Tanes reservoir by using a hybrid WOA optimized SVR-relied technique along with feature selection based on the MARS approximation. – Stoch Environ Res Risk Assess 36: 2561-2580. https://doi.org/10.1007/s00477-021-02136-4.

http://www.aloki.hu ● ISSN 1589 1623 (Print) ● ISSN 1785 0037 (Online)
DOI: http://dx.doi.org/10.15666/aeer/2305_90759099

[18] Hasan, I. F., Abdullah, R. (2022): Agricultural drought characteristics analysis using Copula. – Water Resources Management 36(15): 5915-5930. https://doi.org/10.1007/s11269-022-03331-w.
[19] Hei, P., Yang, T., Huang, L., Liu, Y., Yang, J., Shang, Y., Feng, L., Huang, G. (2024): Unraveling eutrophication controversies: Innovative strategies and holistic perspectives. – Critical Reviews in Environmental Science and Technology 55(3): 147-168. https://doi.org/10.1080/10643389.2024.2392987.
[20] Heredia-Zavoni, E., Montes-Iturrizaga, R. (2022): Environmental contours using nonparametric copulas. – Ocean Engineering 266: 112971. https://doi.org/10.1016/j.oceaneng.2022.112971.
[21] Hochrainer-Stigler, S., Pflug, G., Dieckmann, U., Rovenskaya, E., Thurner, S., Poledna, S., Boza, G., Linnerooth-Bayer, J., Brännström, Å. (2018): Integrating systemic risk and risk analysis using copulas. – International Journal of Disaster Risk Science 9: 561-567. https://doi.org/10.1007/s13753-018-0198-1.
[22] Hou, J. (2013): Water quality parameters characteristics and inversion of Erlong Lake. – Northeast Normal University.
[23] Hou, L., Ma, A., Hu, J., Shan, G., Deng, J., Han, J., Ding, Z. (2018): Study on remote sensing retrieval model optimization of suspended sediment concentration in Jiaozhou Bay. – Periodical of Ocean University of China 48(10): 98-108.
[24] Joe, H. (1996): Families of m-variate distributions with given margins and m(m-1)/2 bivariate dependence parameters. – Institute of Mathematical Statistics, California.
[25] Kanthavel, P., Saxena, C. K., Singh, R. K. (2022): Integrated drought index based on vine copula modelling. – International Journal of Climatology 42: 9510-9529. https://doi.org/10.1002/joc.7840.
[26] Li, Y., Huang, J., Wei, Y., Lu, W., Shi, J. (2006): Evaluating Eutrophic State of Taihu Lake by in situ Hyperspectral. – Environmental Science 9: 1770-1775.
[27] Li, S., Song, K., Wang, S., Liu, G., Wen, Z., Shang, Y., Lyu, L., Chen, F., Xu, S., Tao, H., Du, Y., Fang, C., Mu, G. (2021): Quantification of chlorophyll-a in typical lakes across China using Sentinel-2 MSI imagery with machine learning algorithm. – Science of The Total Environment 778: 146271.
[28] Li, J. (2022): Remote sensing inversion and time-series analysis of critical parameters for eutrophication assessment of urban waters in Shanghai. – Journal of East China Normal University (Natural Science) 1: 135-147.
[29] Li, H., Guo, J., Yan, D., Wang, H., Jiang, X. (2024): Hydrological Drought Risk Assessment and Its Spatial Transmission Based on the Three-Dimensional Copula Function in the Yellow River Basin. – Water 16: 1873. https://doi.org/10.3390/w16131873.
[30] Li, R., Xiao, K., Zhao, G., Huang, X., Zheng, L., Wu, H., Huang, X., Pan, Y., Liang, L. (2024): Comprehensive Assessment of Eutrophication and the Mechanisms Driving Phytoplankton Blooms in Multifunctional Reservoirs. – Water 16: 1752. https://doi.org/10.3390/w16121752.
[31] Liu, X. (2023): Study on Inversion Model of Suspended Matter Concentration in Chagan Lake Based on Multisource Remote Sensing Data. – Jilin University.
[32] Luo, Q., Liu, X., Wang, K., Liu, C. (2024): Increasingly frequent co-occurrence of drought or pluvial in multiple tributaries of the Yangtze River basin. – Journal of Hydrology 633: 131035. https://doi.org/10.1016/j.jhydrol.2024.131035.
[33] Mamun, M., Hasan, M., An, K. (2024): Advancing reservoirs water quality parameters estimation using Sentinel-2 and Landsat-8 satellite data with machine learning approaches. – Ecological Informatics 81: 102608.
[34] Meimandi, J. B., Bazrafshan, O., Esmaeilpour, Y., Zamani, H., Shekari, M. (2024): Risk assessment of meteo-groundwater drought using copula approach in the arid region. – Stoch Environ Res Risk Assess 38: 1523-1540. https://doi.org/10.1007/s00477-023-02641-8.

http://www.aloki.hu ● ISSN 1589 1623 (Print) ● ISSN 1785 0037 (Online)
DOI: http://dx.doi.org/10.15666/aeer/2305_90759099

[35] Mundahl, N. D., Hoisington, J. (2021): Game fish response to dredging of a eutrophic urban lake in Minnesota. – Lake Reserv. Manag. 37: 170-185.
[36] Murakami, K. (1984): Dredging for controlling eutrophication of Lake Kasumigaura, Japan. – Lake Reserv. Manag. 1: 592-598.
[37] Nguyen, D. D., Jayakumar, K. V. (2018): Assessing the copula selection for bivariate frequency analysis based on the tail dependence test. – Journal of Earth System Science 127: 1-17. https://doi.org/10.1007/s12040-018-0994-4.
[38] Niu, C., Tan, K., Wang, X., Du, P., Pan, C. (2024): A semi-analytical approach for estimating inland water inherent optical properties and chlorophyll a using airborne hyperspectral imagery. – International Journal of Applied Earth Observation and Geoinformation 128: 103774. https://doi.org/10.1016/j.jag.2024.103774.
[39] Njock, P. G. A., Zhou, A., Yin, Z., Shen, S. (2023): Integrated risk assessment approach for eutrophication in coastal waters: Case of Baltic Sea. – Journal of Cleaner Production 387: 135673. https://doi.org/10.1016/j.jclepro.2022.135673.
[40] Nõges, P., Argillier, C., Borja, Á., Garmendia, J. M., Hanganu, J., Kodeš, V., Pletterbauer, F., Sagouis, A., Birk, S. (2016): Quantified biotic and abiotic responses to multiple stress in freshwater, marine and ground waters. – Science of The Total Environment 540: 43-52.
[41] Ogashawara, I., Moreno-Madriñán, M. J. (2014): Improving Inland Water Quality Monitoring through Remote Sensing Techniques. – ISPRS International Journal of Geo-Information 3(4): 1234-1255.
[42] Pahlevan, N., Lee, Z., Wei, J., Schaaf, C. B., Schott, J. R., Berk, A. (2014): On-orbit radiometric characterization of OLI (Landsat-8) for applications in aquatic remote sensing. – Remote Sensing of Environment 154: 272-284.
[43] Pannard, A., Souchu, P., Chauvin, C., Delabuis, M., Gascuel-Odoux, C., Jeppesen, E., Moal, M. L., Ménesguen, A., Pinay, G., Rabalais, N. N., Souchon, Y., Gross, E. M. (2024): Why are there so Many Definitions of Eutrophication? – Ecological Monographs 94(3): e1616. https://doi.org/10.1002/ecm.1616.
[44] Qi, Y., Cao, X., Cao, R., Cao, M., Yan, A., Li, E., Xu, D. (2024): Research on the Analysis of and Countermeasures for the Eutrophication of Water Bodies: Waihu Reservoir as a Case Study. – Processes 12(4): 796.
[45] Qian, L., Wang, X., Wang, Z. (2020): Modeling the dependence pattern between two precipitation variables using a coupled Copula. – Environmental Earth Sciences 79: 1-12. https://doi.org/10.1007/s12665-020-09233-7.
[46] Qian, R., Peng, F., Xue, K., Qi, L., Duan, H., Qiu, Y., Chen, Q., Chen, F., Gao, J., Huang, J. (2022): Assessing the risks of harmful algal bloom accumulation at littoral zone of large lakes and reservoirs: An example from Lake Chaohu. – Journal of Lake Sciences 34(01): 49-60.
[47] Qu, W., Wang, Y., Wang, L., Li, J., Li, D. (2024): An feature optimization selection method of SEaTH considering discretization degree. – Acta Geodaetica et Cartographica Sinica 53(1): 20-35.
[48] Saravani, M. J., Noori, R., Jun, C., Kim, D., Bateni, S. M., Kianmehr, P., Woolway, R. L. (2025): Predicting Chlorophyll-a Concentrations in the World's Largest Lakes Using Kolmogorov-Arnold Networks. – Environmental Science & Technology 59(3): 1801-1810. https://doi.org/10.1021/acs.est.4c11113.
[49] Shih, J. H., Louis, T. A. (1995): Inferences on the association parameter in copula models for bivariate survival data. – Biometrics 51(4): 1384-1399. https://doi.org/10.2307/2533269.
[50] Sklar, M. (1959): Fonctions de répartition à n dimensions et leurs marges. – Publications de l'Institut Statistique de l'Université de Paris 8(3): 229-231.
[51] Sun, Y., Wang, D., Li, L., Ning, R., Yu, S., Gao, N. (2024): Application of remote sensing technology in water quality monitoring: From traditional approaches to artificial intelligence. – Water Research 267: 122546. https://doi.org/10.1016/j.watres.2024.122546.

http://www.aloki.hu ● ISSN 1589 1623 (Print) ● ISSN 1785 0037 (Online)
DOI: http://dx.doi.org/10.15666/aeer/2305_90759099

[52] Tian, P., Xu, Z., Fan, W., Lai, H., Liu, Y., Yang, P., Yang, Z. (2024): Exploring the effects of climate change and urban policies on lake water quality using remote sensing and explainable artificial intelligence. – Journal of Cleaner Production 475: 143649.
[53] Tosunoglu, F., Gürbüz, F., İspirli, M. N. (2020): Multivariate modeling of flood characteristics using Vine copulas. – Environmental Earth Sciences 79: 1-21. https://doi.org/10.1007/s12665-020-09199-6.
[54] Vasilakou, K., Nimmegeers, P., Yao, Y., Billen, P., Passel, S. V. (2025): Global spatiotemporal characterization factors for freshwater eutrophication under climate change scenarios. – Science of The Total Environment 959: 178275. https://doi.org/10.1016/j.scitotenv.2024.178275.
[55] Wang, J., Xu, C. (2017): Geodetector: Principle and prospective. – Acta Geographica Sinica 72(1): 116-134.
[56] Wang, S., Zhang, R., Guo, L., Xu, L., Chen, C., Lu, S., Wang, X. (2017): Study on the water ecological risk prevention and control technology system of Dongting lake. – China Environmental Science 37(5): 1896-1905.
[57] Wang, L., Shao, H., Guo, Y., Bi, H., Lei, X., Dai, S., Mao, X., Xiao, K., Liao, X., Xue, H. (2024): Ecological restoration for eutrophication mitigation in urban interconnected water bodies: Evaluation, variability and strategy. – Journal of Environmental Management 365: 121475. https://doi.org/10.1016/j.jenvman.2024.121475.
[58] Wang, H., Liu, C., Li, L., Kong, Y., Akbar, A., Zhou, X. (2025): High-precision inversion of urban river water quality via integration of riparian spatial structures and river spectral signatures. – Water Research 278: 123378. https://doi.org/10.1016/j.watres.2025.123378.
[59] Wen, S., Wang, Q., Li, Y., Zhu, L., Lyu, H., Lei, S., Ding, X., Miao, S. (2018): Remote sensing identification of urban black-odor water bodies based on high-resolution images: a case study in Nanjing. – Environmental Science 39(1): 57-67.
[60] Wen, C., Zhou, Z., Li, Y., Kong, J., Xie, J. (2023): Remote sensing retrieval of water transparency for Pingzhai reservoir based on Sentinel-2 images. – Bulletin of Soil and Water Conservation 43(1): 158-166.
[61] Wu, H., Wang, R., Yan, P., Wu, S., Chen, Z., Zhao, Y., Cheng, C., Hu, Z., Zhuang, L., Guo, Z. (2023): Constructed wetlands for pollution control. – Nat. Rev. Earth Environ. 4: 218-234.
[62] Yao, Y., Shen, Q., Zhu, L., Gao, H., Cao, H., Han, H., Sun, J., Li, J. (2019): Remote sensing identification of urban black-odor water bodies in Shenyang city based on GF-2 image. – Journal of Remote Sensing 23(2): 230-242.
[63] Zhang, R., Zeng, F., Liu, W., Zeng, R., Jiang, H. (2014): Precise and economical dredging model of sediments and its field application: Case study of a river heavily polluted by organic matter, nitrogen, and phosphorus. – Environ. Manag. 53: 1119-1131.
[64] Zhang, X., Jiang, H. (2019): Application of Copula function in financial risk analysis. – Computers & Electrical Engineering 77: 376-388. https://doi.org/10.1016/j.compeleceng.2019.06.011.
[65] Zhang, J., Cai, Q., Kang, Z., Cong, M., Han, L., He, J., Yang, L. (2025): Analysis, Evaluation, and Prediction Model of Water Quality in the Weihe River Basin. – Environmental Science. https://doi.org/10.13227/j.hjkx.202408033.
[66] Zhao, M., Jiao, S., Liang, H. (2020): Eutrophication of Lakes in Karst Plateau Based on the Comprehensive Trophic State Index Method. – Journal of China Hydrology 40(3): 9-15.
[67] Zhu, L., Li, Y., Zhao, S., Guo, Y. (2015): Remote sensing monitoring of Taihu Lake water quality by using GF-1 satellite WFV data. – Remote Sensing for Land and Resources 27(1): 113-120.
[68] Zill, J., Perujo, N., Fink, P., Mallast, U., Siebert, C., Weitere, M. (2024): Contribution of groundwater-borne nutrients to eutrophication potential and the share of benthic algae in a large lowland river. – Science of The Total Environment 951: 175617. https://doi.org/10.1016/j.scitotenv.2024.175617.

http://www.aloki.hu ● ISSN 1589 1623 (Print) ● ISSN 1785 0037 (Online)
DOI: http://dx.doi.org/10.15666/aeer/2305_90759099

[69] Zimba, P. V., Gitelson, A. (2006): Remote estimation of chlorophyll concentration in hyper-eutrophic aquatic systems: Model tuning and accuracy optimization. – Aquaculture 256: 272-286.

http://www.aloki.hu ● ISSN 1589 1623 (Print) ● ISSN 1785 0037 (Online)
DOI: http://dx.doi.org/10.15666/aeer/2305_90759099